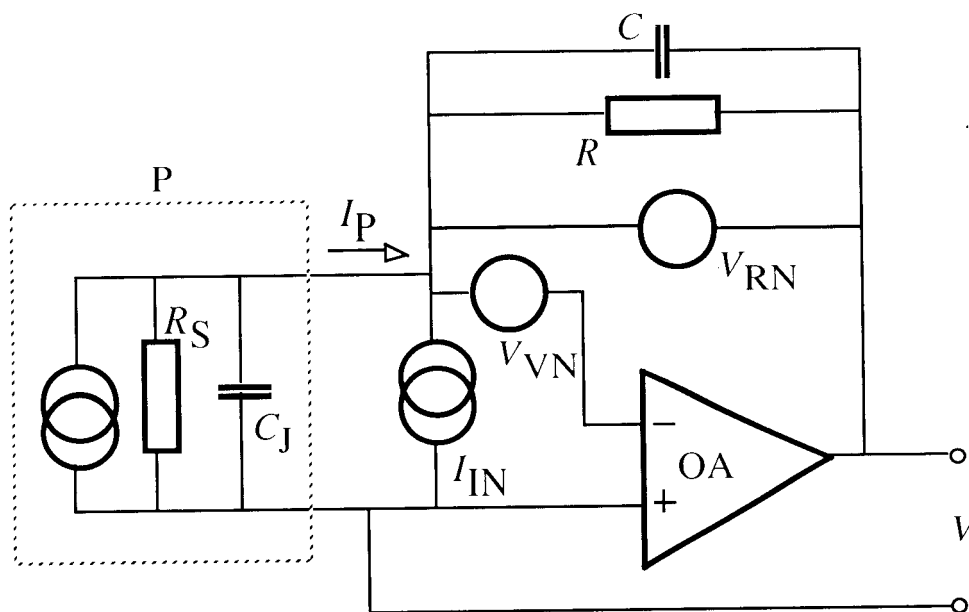


# Optical Radiation Measurement with Selected Detectors and Matched Electronic Circuits Between 200 nm and 20 $\mu\text{m}$

George P. Eppeldauer, Editor



**T**he National Institute of Standards and Technology was established in 1988 by Congress to “assist industry in the development of technology . . . needed to improve product quality, to modernize manufacturing processes, to ensure product reliability . . . and to facilitate rapid commercialization . . . of products based on new scientific discoveries.”

NIST, originally founded as the National Bureau of Standards in 1901, works to strengthen U.S. industry’s competitiveness; advance science and engineering; and improve public health, safety, and the environment. One of the agency’s basic functions is to develop, maintain, and retain custody of the national standards of measurement, and provide the means and methods for comparing standards used in science, engineering, manufacturing, commerce, industry, and education with the standards adopted or recognized by the Federal Government.

As an agency of the U.S. Commerce Department’s Technology Administration, NIST conducts basic and applied research in the physical sciences and engineering, and develops measurement techniques, test methods, standards, and related services. The Institute does generic and precompetitive work on new and advanced technologies. NIST’s research facilities are located at Gaithersburg, MD 20899, and at Boulder, CO 80303. Major technical operating units and their principal activities are listed below. For more information contact the Publications and Program Inquiries Desk, 301-975-3058.

---

### **Office of the Director**

- National Quality Program
- International and Academic Affairs

### **Technology Services**

- Standards Services
- Technology Partnerships
- Measurement Services
- Information Services

### **Advanced Technology Program**

- Economic Assessment
- Information Technology and Applications
- Chemistry and Life Sciences
- Materials and Manufacturing Technology
- Electronics and Photonics Technology

### **Manufacturing Extension Partnership Program**

- Regional Programs
- National Programs
- Program Development

### **Electronics and Electrical Engineering Laboratory**

- Microelectronics
- Law Enforcement Standards
- Electricity
- Semiconductor Electronics
- Radio-Frequency Technology<sup>1</sup>
- Electromagnetic Technology<sup>1</sup>
- Optoelectronics<sup>1</sup>

### **Materials Science and Engineering Laboratory**

- Intelligent Processing of Materials
- Ceramics
- Materials Reliability<sup>1</sup>
- Polymers
- Metallurgy
- NIST Center for Neutron Research

### **Chemical Science and Technology Laboratory**

- Biotechnology
- Physical and Chemical Properties<sup>2</sup>
- Analytical Chemistry
- Process Measurements
- Surface and Microanalysis Science

### **Physics Laboratory**

- Electron and Optical Physics
- Atomic Physics
- Optical Technology
- Ionizing Radiation
- Time and Frequency<sup>1</sup>
- Quantum Physics<sup>1</sup>

### **Manufacturing Engineering Laboratory**

- Precision Engineering
- Manufacturing Metrology
- Intelligent Systems
- Fabrication Technology
- Manufacturing Systems Integration

### **Building and Fire Research Laboratory**

- Applied Economics
- Structures
- Building Materials
- Building Environment
- Fire Safety Engineering
- Fire Science

### **Information Technology Laboratory**

- Mathematical and Computational Sciences<sup>2</sup>
- Advanced Network Technologies
- Computer Security
- Information Access
- Convergent Information Systems
- Information Services and Computing
- Software Diagnostics and Conformance Testing
- Statistical Engineering

---

<sup>1</sup>At Boulder, CO 80303.

<sup>2</sup>Some elements at Boulder, CO.

# **Optical Radiation Measurement with Selected Detectors and Matched Electronic Circuits Between 200 nm and 20 $\mu\text{m}$**

---

George P. Eppeldauer, Editor  
Optical Technology Division  
Physics Laboratory  
National Institute of Standards and Technology  
Gaithersburg, MD 20899-8440

April 2001



U.S. Department of Commerce  
*Donald L. Evans, Secretary*

Technology Administration  
*Dr. Karen H. Brown, Acting Under Secretary of Commerce for Technology*

National Institute of Standards and Technology  
*Dr. Karen H. Brown, Acting Under Secretary of Commerce for Technology*

Certain commercial entities, equipment, or materials may be identified in this document in order to describe an experimental procedure or concept adequately. Such identification is not intended to imply recommendation or endorsement by the National Institute of Standards and Technology, nor is it intended to imply that the entities, materials, or equipment are necessarily the best available for the purpose.

**Front Cover:**

Equivalent circuit of a photodiode current-meter. The feedback impedance,  $R$  and  $C$ , of an operational amplifier, OA, converts the photocurrent  $I_P$  of photodiode P into a voltage  $V$ .  $R$  and  $C$  together with the impedance of the photodiode,  $R_S$  and  $C_J$ , attenuate  $V$  to the OA input. The inverse of this feedback attenuation is the (closed-loop) voltage gain for the OA input drift and noise. Single circles illustrate voltage sources and double circles illustrate current sources. One signal (the photocurrent) source and three noise sources are shown in the circuit. The product of the feedback attenuation and the OA open-loop gain gives the loop gain that determines the uncertainty of the photocurrent-to-voltage conversion at a given signal frequency. Design considerations and performance evaluation of photodiode current-meters are discussed in Papers 1, 3 and 4 for Si photodiodes, in Paper 5 for Si trap detectors, in Paper 6 for Ge and InGaAs photodiodes, and in Paper 7 for InSb photodiodes.

---

National Institute of Standards  
and Technology  
Technical Note 1438  
Natl. Inst. Stand. Technol.  
Tech. Note 1438  
117 pages (April 2001)  
CODEN: NTNOEF

U.S. Government Printing Office  
Washington: 2001

For Sale by the  
Superintendent of Documents  
U.S. Government Printing Office  
Internet: bookstore.gpo.gov  
Phone: (202) 512-1800  
Fax: (202) 512-2250  
Mail: Stop SSOP, Washington, DC  
20402-0001

## Preface

Improved detector technology in the past decade opened a new era in the field of radiometric and photometric calibrations. Now, cryogenic electrical substitution radiometers with 0.01 % optical power measurement uncertainty are the primary standards of the field. New generation radiometers, built with high electronic and radiometric performance detectors, became the transfer and working standards to propagate the high accuracy from the primary standard to field level measurements. The importance of high quality detector standards has greatly increased as a result of demands in a wide range of technical areas. Nowadays, lamp standards, traditionally calibrated against source standards, are calibrated against detector standards to obtain improved calibration accuracy.

The purpose of this Technical Note is to summarize the results of the research and development work carried out at the Optical Sensor Group of the Optical Technology Division for constructing accurate and wide dynamic range radiometers with high performance detectors for the 200 nm to 20  $\mu\text{m}$  wavelength range. Linear and stable operation was required from these radiometers to achieve detector spectral responsivity transfer with low uncertainty. Large area thermal, pyroelectric, photoconductive (PC), and photovoltaic (PV) detectors were selected, applied, and characterized at different controlled temperatures between 4.2 K and 300 K. The resistance of these detectors ranged from 15  $\Omega$  to 50 G $\Omega$ , their capacitance ranged from 0.18 nF to 36 nF. The detector output-signal measuring electronic circuits had to be designed and individually matched to the complex impedance of the selected detector to optimize radiometer performance. The frequency dependent fundamental gain-equations of operational-amplifier photocurrent-meters have been worked out and applied for a large number of different types of photodiodes operating in both dc and ac signal measurement modes. The gain equations were utilized to achieve signal measurement uncertainties between 0.1 % and 0.01 % . Drift and noise were minimized for the radiometer outputs to obtain high signal-to-noise ratios even at high signal gains.

The NIST developed radiometer standards are the key components of several recently realized high accuracy scales. These are the spectral power and irradiance responsivity scales on the Spectral Comparator Facilities (for the ultraviolet, visible, and infrared ranges), the spectral power, irradiance, and radiance responsivity scales of the Spectral Irradiance and Radiance Responsivity Calibrations with Uniform Sources Facility (SIRCUS), the detector-based illuminance (photometric) scale, and the spectral irradiance scale (disseminated by lamps).

Related additional papers, describing the input geometry, electronic and radiometric characterizations, and spectral responsivity calibrations of the transfer and working standard radiometers are not included here. These subjects are beyond the scope of this Technical Note.

George P Eppeldauer  
Ph.D. Electronics Engineer  
Radiometer and Calibration Development  
Optical Sensors Group, Optical Technology Division  
National Institute of Standards and Technology  
100 Bureau Drive, Gaithersburg, MD 20899-8441

# Table of Contents

Preface.....	iii
Introduction to the papers.....	vii
1. "Fourteen-decade photocurrent measurements with large-area silicon photodiodes at room temperature," Applied Optics, Vol. 30, No.22. 3091-3099, 1991. G. Eppeldauer and J. E. Hardis .....	1
2. "Temperature Monitored/Controlled Silicon Photodiodes for Standardization," SPIE Proceedings, Vol. 1479, 71-77, 1991. G. Eppeldauer.....	11
3. "Chopped Radiation Measurement With Large Area Si Photodiodes," Journal of Research of the National Institute of Standards and Technology, Vol. 103, No. 2, 153-162, 1998. G. P. Eppeldauer.....	19
4. "Noise-optimized silicon radiometers," J. Res. Natl. Inst. Stand. Technol. Vol. 105, No. 209, 209-219, 2000. G. Eppeldauer .....	29
5. "Opto-mechanical and electronic design of a tunnel-trap Si-radiometer," to be published in the J. Res. Natl. Inst. Stand. Technol. G. P. Eppeldauer and D. C. Lynch .....	41
6. "Electronic characteristics of Ge and InGaAs radiometers," SPIE, Proceedings, Vol. 3061-97, 833-838, 1997. G. Eppeldauer. ....	63
7. "InSb Working Standard Radiometers," Metrologia, Vol. 35, 485-490, 1998. G. P. Eppeldauer, A. L. Migdall, and L. M. Hanssen .....	69
8. "Domain-engineered pyroelectric radiometer," Applied Optics, Vol. 38, No. 34, 7047-7055, 1999. J. Lehman, G. Eppeldauer, J. A. Aust, and M. Racz.....	75
9. "A cryogenic silicon resistance bolometer for use as an infrared transfer standard detector," in <i>Thermal Phenomena at Molecular and in Cryogenic Infrared Detectors</i> , M. Kaviani, D. A. Kaminski, A. Majumdar, P. E. Phelan, M. M. Yovanovich, and Z. M. Zhang, eds., book H00908-1994 (American Society of Mechanical Engineers, New York), pp. 63-67. G. Eppeldauer, A. L. Migdall, and C. L. Cromer.....	85
10. "Linear HgCdTe radiometer," SPIE Proceedings, Vol. 1110, 267-273, 1989. G. Eppeldauer and L. Novak .....	91
11. "Photocurrent measurement of PC and PV HgCdTe detectors," to be published in the J. Res. NIST. G. P. Eppeldauer and R. J. Martin.....	99

## Introduction to the Papers

George P. Eppeldauer

### Paper 1

**“Fourteen-decade photocurrent measurements with large-area silicon photodiodes at room temperature,”** *Applied Optics*, Vol. 30, No.22. 3091-3099, 1991. G. Eppeldauer and J. E. Hardis

The noise and drift characteristics of large area silicon photodiode current meters are analyzed at low (dc) frequencies in this paper. High shunt-resistance silicon photodiodes and operational amplifiers with large feedback resistors were used to achieve high photocurrent sensitivity at room temperature. Operational amplifiers with very low input-bias-current were selected to minimize  $1/f$  noise from the amplifier. The dominant resistor noise was equalized to the  $1/f$  amplifier noise by decreasing the electrical bandwidth to 1.25 mHz. The drift was also equalized to the noise floor by regulating the temperature of the Si radiometer within  $\pm 0.02$  °C of the operating 25 °C value. The equivalent photocurrent of the measured noise floor was  $10^{-16}$  A at a measurement time of 400 s. This implies a signal measurement range of 14 decades. When the bandwidth was increased to 0.3 Hz, the noise increased and ranged between 0.6 fA and 1 fA.

### Paper 2

**“Temperature Monitored/Controlled Silicon Photodiodes for Standardization,”** *SPIE Proceedings*, Vol. 1479, 71-77, 1991. G. Eppeldauer

The paper describes how to monitor or control the temperature of photodiodes to obtain improved accuracy in photocurrent measurements. Temperature monitored detectors are easier to construct, but they require more calibration data and analysis as well as additional steps to interpret the results of measurements. Temperature regulated detectors make measurement taking simpler, with the expenses of additional and more complex hardware. Design considerations and examples for both methods are described.

### Paper 3

**“Chopped Radiation Measurement With Large Area Si Photodiodes,”** *Journal of Research of the National Institute of Standards and Technology*, Vol. 103, No. 2, 153-162, 1998. G. P. Eppeldauer

The different frequency-dependent gains of photodiode current meters were analyzed in this paper. The gain equations are needed to perform constant (flat) signal-gains up to a high enough roll-off frequency, to understand and minimize the noise-boosting effect with increasing frequencies (this caused the factor of 10 noise increase in Paper 1), and to achieve small uncertainties in the current-to-voltage conversions. The different gain characteristics were illustrated with Bode plots. The Bode plots were made from the gain equations using spread-sheets. Computer simulators were not used. Signal-gain dependent frequency compensations were applied to optimize dc and ac photocurrent measurements with large area Si photodiodes.

### Paper 4

**“Noise-optimized silicon radiometers,”** *J. Res. Natl. Inst. Stand. Technol.* Vol. 105, No. 209, 209-219, 2000. G. Eppeldauer

This paper is an extension of Paper 3. In addition to the design considerations of the dynamic (frequency dependent) characteristics of photodiode current meters, an experimentally verified noise

analysis is described. After optimizing the dynamic characteristics, the noise floor was minimized in an ac measurement mode using Si photodiodes of different shunt resistance and operational amplifiers with low  $1/f$  voltage and current noise. An equivalent root-mean-square (rms) photocurrent noise of  $8 \times 10^{-17}$  A was performed at a 9 Hz chopping frequency and 30 s integration time constant. The radiometers, optimized for ac measurements, were tested in a dc measurement mode as well. Performances in ac and dc measurement modes were compared. In the ac mode, a ten times shorter (40 s) overall measurement time was needed than in the dc mode (described in Paper 1) to obtain the same  $10^{-16}$  A noise floor.

#### Paper 5

**“Opto-mechanical and electronic design of a tunnel-trap Si-radiometer,” to be published in the J. Res. Natl. Inst. Stand. Technol. G. P. Eppeldauer and D. C. Lynch**

The design methods described in Papers 3 and 4 were applied to a transmission-type light-trap silicon detector. Six Si photodiodes of two different sizes, selected for equal shunt resistance, were connected in parallel in this power/irradiance mode transfer standard. The capacitance and the resultant shunt resistance of the device were measured and frequency compensations were applied in the feedback network of the photocurrent-to-voltage converter to optimize signal-, voltage-, and loop-gain characteristics. The trap-radiometer can measure either dc or ac optical radiation with high sensitivity. The noise-equivalent power of the optimized device was 47 fW in dc mode and 5.2 fW at 10 Hz chopping. The deviation from the cosine responsivity in irradiance mode was measured to be equal to or less than 0.02 % within  $5^\circ$  FOV and 0.05 % at  $8^\circ$  FOV. Both the electronic and the optical-mechanical design considerations are discussed in detail.

#### Paper 6

**“Electronic characteristics of Ge and InGaAs radiometers,” SPIE, Proceedings, Vol. 3061-97, 833-838, 1997. G. Eppeldauer**

Equal size (5 mm diameter) Ge and InGaAs photodiodes were tested in NIST-developed radiometers and compared for sensitivity and stability. The electronic characteristics of the radiometers were measured versus photodiode temperature with a bandwidth of 0.3 Hz. At  $-30^\circ\text{C}$ , a limit-sensitivity of 22 fA and a dark-current stability of 0.2 pA/16 hours were achieved with the InGaAs radiometer, which was three times better than the results obtained with the Ge radiometer. The frequency dependent gain characteristics were calculated and compared for the two types of radiometer as well. The 36 nF capacitance of the Ge photodiode caused a noise boosting effect (voltage-gain increase) for frequencies higher than 0.3 Hz. Accordingly, the Ge radiometer was restricted for dc signal measurements only. The 0.5 nF capacitance of the InGaAs photodiode did not produce any noise boosting up to about 8 Hz. The  $10^4$  loop gain at 8 Hz resulted in a 0.01% (coverage factor  $k=1$ ) current-to-voltage conversion uncertainty. The InGaAs radiometer could measure an 80 Hz signal with a relative uncertainty of 0.1 % ( $k=1$ ).

#### Paper 7

**“InSb Working Standard Radiometers,” Metrologia, Vol. 35, 485-490, 1998. G. P. Eppeldauer, A. L. Migdall, and L. M. Hanssen**

Characterization of custom-made transfer standard InSb radiometers is described in this paper. The InSb radiometers maintain the spectral radiant power and irradiance responsivity scales of NIST between  $2 \mu\text{m}$  and  $5.4 \mu\text{m}$ . The field-of-view of the 77 K detectors is limited to  $17^\circ$ . The InSb detectors were selected for high shunt impedance to achieve high sensitivity. The transimpedance-,

voltage-, and loop-gains of the current-to-voltage converters were optimized for optical radiation chopped at 40 Hz. At the peak responsivity, the noise-equivalent-power (NEP) is 0.6 pW in an electrical bandwidth of 0.3 Hz. The ratio of the dc ambient-background-current to the ac noise-equivalent-current is  $10^7$ . Spatial and angular responsivities, linearity, stability, and flashing were also characterized.

#### Paper 8

**“Domain-engineered pyroelectric radiometer,” *Applied Optics*, Vol. 38, No. 34, 7047-7055, 1999. J. Lehman, G. Eppeldauer, J. A. Aust, and M. Racz**

A domain-engineered pyroelectric transfer standard radiometer has been developed at NIST to extend the spectral responsivity scale from the visible to the ultraviolet and near-infrared ranges. The domain engineering consisted of inverting the spontaneous polarization over a 10 mm diameter area in the center of a uniformly poled, 15.5 mm x 15.5 mm square, 0.25 mm thick LiNbO<sub>3</sub> plate. Gold black was used as the optical absorber on the detector surface, and an aperture was added to define the optically sensitive detector area. The radiometer included a temperature monitor for the detector and a current-to-voltage converter optimized for signal- and loop-gain. The results indicate that the acoustic sensitivity was significantly reduced without loss of optical sensitivity. The detector noise-equivalent-power was not exceptionally low but was nearly constant for different acoustic backgrounds. In addition, the detector's spatial response uniformity variation was less than 0.1 % across the 7.5 mm diameter aperture, and reflectance measurements indicated that the gold black coating was spectrally uniform, within 0.2 %, from 800 nm to 1800 nm. Other detailed evaluations of the radiometer include detector responsivity as a function of temperature, electrical frequency response, angular response, and field of view.

#### Paper 9

**“A cryogenic silicon resistance bolometer for use as an infrared transfer standard detector,” in *Thermal Phenomena at Molecular and in Cryogenic Infrared Detectors*, M. Kaviany, D. A. Kaminski, A. Majumdar, P. E. Phelan, M. M. Yovanovich, and Z. M. Zhang, eds., book H00908-1994 (American Society of Mechanical Engineers, New York), pp. 63-67. G. Eppeldauer, A. L. Migdall, and C. L. Cromer**

A transfer standard cryogenic bolometer has been developed to maintain the NIST spectral power responsivity scale between 2  $\mu\text{m}$  and 20  $\mu\text{m}$ . The resistance of the heavily doped Si sensor increased six orders of magnitude when it was cooled down from room temperature to the 4.2 K operating temperature. The computer controlled bolometer has high sensitivity, accuracy, stability and dynamic range as well as a large detector area, fast time response and flat spectral response. The design and testing of the silicon composite bolometer is described in this paper. This device has a dynamic range of 5 decades, a noise floor of 36 pW/Hz<sup>1/2</sup>, a nonlinearity of less than 1%, a spatial response nonuniformity of about 0.3% and a constant frequency-dependent response out to about 100 Hz.

#### Paper 10

**“Linear HgCdTe radiometer,” *SPIE Proceedings*, Vol. 1110, 267-273, 1989. G. Eppeldauer and L. Novak**

The basic modes of electrical operation of photoconductive optical radiation detectors are analyzed in this paper. The nonlinearity in voltage-mode measurements can be eliminated by using current-mode measurements. A HgCdTe photoconductive radiometer has been designed, based on this analysis,

which measures the current through a biased detector. A built-in calibrating capability in the circuits of the radiometer makes it possible to eliminate the effects of a long-term drift in the bias voltage, thereby achieving a lower uncertainty.

Paper 11

**“Photocurrent measurement of PC and PV HgCdTe detectors,” to be published in the J. Res. NIST. G. P. Eppeldauer and R. J. Martin**

Novel photocurrent meters for working standard photoconductive (PC) and photovoltaic (PV) HgCdTe detectors have been developed to maintain the spectral responsivity scale of NIST in the wavelength range of 5  $\mu\text{m}$  to 20  $\mu\text{m}$ . The linear PC mode preamplifier does not need any compensating source to zero the effect of the detector bias current for the preamplifier output. The impedance multiplication concept with a positive feedback buffer amplifier was analyzed and utilized in a bootstrap transimpedance amplifier to measure photocurrent of a 200  $\Omega$  shunt resistance photodiode with a maximum signal gain of  $10^8$  V/A. In spite of the high performance lock-in used as a second-stage signal-amplifier, the signal-to-noise ratio had to be optimized for the output of the photocurrent preamplifiers. Noise and drift were equalized for the output of the PV mode preamplifier. The signal gain errors were calculated to determine the signal frequency range where photocurrent-to-voltage conversion can be performed with very low uncertainties. For the design of both PC and PV detector preamplifiers, the most important gain equations are described. Measurement results on signal ranges and noise performance are discussed.

# Fourteen-decade photocurrent measurements with large-area silicon photodiodes at room temperature

G. Eppeldauer and J. E. Hardis

Recent improvements in commercial silicon photodiodes and operational amplifiers permit electrical noise to be reduced to an equivalent of 0.1 fA of photocurrent when a measurement time of 400 s is used. This is equivalent to a photocurrent resulting from fewer than 800 photons/s, and it implies a dynamic range of 14 orders of magnitude for a detector circuit. We explain the circuit theory, paying particular attention to the measurement bandwidth, the causes of noise and drift, and the proper selection of circuit components. These optical radiation detectors complement the primary radiometric standards. These detectors may replace photomultiplier tubes that have been used traditionally and or that were too costly to be used.

*Key words:* Bandwidth, dynamic range, noise, optical detection, photodiode, photonics, radiometry, sensitivity.

## I. Introduction

The improvements in commercial silicon photodiodes and operational amplifiers over the past several years permit a corresponding increase in the performance of optical radiation measurements. Important electrical properties of photodiodes and operational amplifiers that affect high-sensitivity applications have been reported in the literature.<sup>1</sup> A limiting factor is the  $1/f$  noise of the operational amplifier, which is chosen to be an electrometer-grade device characterized by a high input impedance and a low input bias current. Another limiting factor is the shunt resistance of the photodiode. This is the effective resistance that connects in parallel to the photocurrent source and is the slope of the diode's I-V curve at the operating point. For the study in Ref. 1 photodiodes were not available with shunt resistances  $>1.4 \text{ G}\Omega$ . More recently, the shunt resistances of the best silicon photodiodes have increased by an order of magnitude. Further, operational amplifiers have become available with an order of magnitude less input noise. These developments

have made it necessary to reanalyze the behavior of these devices in a complete measurement circuit. Our goals in this study were to get optimum performance and to extend the application of these detectors to situations in which greater sensitivity would be required.

There is a growing market for such solid-state detectors. One photodiode manufacturer offers an integrated silicon-photodiode and monolithic-operational-amplifier package with a specification of 5-fW noise equivalent power (NEP) in the band of dc to 1 Hz at 750-nm peak response.<sup>2</sup> The manufacturer uses a small-surface-area ( $6.7 \text{ mm}^2$ ) photodiode and a fixed-gain amplifier of  $10^{10} \text{ V/A}$ . The product literature compares this device with a photomultiplier tube (R374 with an S-20 photocathode), as its NEP is less than the photomultiplier for wavelengths longer than 760 nm.

An intended application of this product is in optical communication, where greater detector sensitivity permits longer ranges. However, there are a large number of other applications in which silicon detectors could replace large and expensive photomultiplier tubes or inspire new, better, or less-expensive products. There is an increasing demand for high-sensitivity radiant-power measurements in such diverse fields as chemiluminescence and bioluminescence, radiometry, photometry, pyrometry, materials science (optical density and surface-scatter measurements), astronomy (Earth- and space-based stellar radiometry), and night vision. Silicon photodiodes offer the additional advantages of higher stability, greater reliability, linearity over a greater dynamic range,<sup>3</sup> and simpler operation.

The authors are with the Radiometric Physics Division, National Institute of Standards and Technology, Gaithersburg, Maryland 20899.

Received 12 October 1990.

0003-6935/91/223091-09\$05.00/0.

© 1991 Optical Society of America.

The field of stellar radiometry illustrates an application for which high stability is as important as high sensitivity. Searching for planets around stars depends on the observance of small decreases in starlight (0.01% for terrestrial-sized planets) produced by the transit of a planet across a stellar disk.<sup>4,5</sup> To measure a  $10^{-4}$  change requires a signal-to-noise ratio of  $10^5$  or better and a correspondingly high stability.

The goals of high sensitivity, wide dynamic range, stability, and linearity complement the silicon photodiode detectors that are used as self-calibrated, primary standards.<sup>6</sup> These photodiodes are inversion-layer silicon devices, which have a limited range of linear operation.<sup>7,8</sup> When they are combined in a light-trap arrangement to eliminate reflectance losses,<sup>9</sup> the range of operation for highest accuracy is further limited to less than a decade. The appropriate radiant power level used in realizing primary standards is a few tenths of a milliwatt, which typically requires a laser light source. However most applications that use traditional light sources and monochromators involve much lower radiant power levels. The silicon photodiode detectors discussed in this paper could act as transfer standards and improve the overall dynamic range of silicon-based radiometric standardization.

## II. Circuit Theory

Consider the basic circuit of Fig. 1(a). The photodiode operates without a bias voltage, in the so-called short-circuit arrangement.<sup>10</sup> The output voltage ( $V_{Out}$ ) of the amplifier is proportional to the photocurrent from the diode, as determined by the feedback transimpedance  $R_f$ . From the viewpoint of the photodiode, the amplifier and the feedback resistor appear as an impedance of  $R_f/A$  across its terminals, where  $A$  is the open-loop gain of the amplifier. As  $A$  is of the order of  $10^6$ , the short-circuit impedance across the photodiode is very small compared with typical values of the photodiode's shunt resistance,  $R_{sh}$ , even when  $R_f$  is of the order of  $10^{11} \Omega$ .

Figure 1(b) emphasizes the aspects of this circuit that contribute to the measurement noise. The amplifier contains two noise sources. The first is  $V_{VN}$ , input voltage noise, which manifests itself as an effective voltage fluctuation at the input terminal of the amplifier.  $V_{VN}$  is the principal source of  $1/f$  noise. That is, it has equal power in each decade of the measurement passband. The other is  $I_{IN}$ , input current noise, which is caused by the fluctuation of the input bias current of the amplifier.  $I_{IN}$  is a white noise, with a power proportional to the bandwidth.

Although ideal operational amplifiers are usually modeled as having a high, if not infinite, input impedance (and nothing more), real ones are the source of a small amount of current at the input pins. This input bias current is of the order of  $10^{-12}$ – $10^{-13}$  A in good devices and may occur with either polarity on a piece-by-piece basis.  $I_{IN}$  is caused by the shot noise of the charge carriers of the input bias current. Current shot noise has the well-known rms value of  $\sqrt{2eI\Delta f}$ , where  $e$  is the charge of the electron and  $\Delta f$  is the frequency

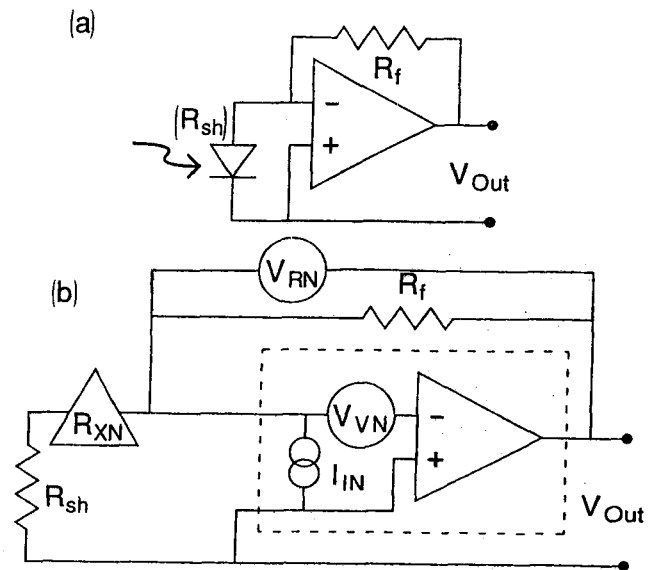


Fig. 1. Model circuit (a) components and (b) noise sources.

bandwidth of the measurement. In a typical operational amplifier with differential inputs, the current fluctuations would be larger. We approximate  $I_{IN}$  as  $(4eI_{Bias}\Delta f)^{1/2}$ .<sup>11</sup>

The effect of  $I_{IN}$  depends on the amplifier's source impedance. In our case, the source resistance,  $R_{so}$ , is the parallel combination of  $R_{sh}$  and  $R_f$  [ $R_{so} = R_{sh} \times R_f / (R_{sh} + R_f)$ ]. The input current noise is reflected as an input voltage on the amplifier of  $I_{IN}R_{so}$ .

In manufacturers' specifications the claim "low noise" usually refers to  $V_{VN}$ . "Low input bias current" implies low  $I_{IN}$ . Choosing which attribute is the most important for a particular application depends on  $R_{so}$ , the bandwidth of the measurement, and the temperature stability of the measuring circuit. This theme is a major purpose of this paper.

Figure 1(b) also illustrates two other noise sources of concern. One is the voltage that is due to resistor noise,  $V_{RN}$ , which is also known as Johnson noise or thermal noise. This noise is an inevitable consequence of charge carriers in resistors. Its rms value is  $(4kTR_{so}\Delta f)^{1/2}$ , where  $k$  is Boltzmann's constant and  $T$  is the absolute temperature.<sup>12</sup> Like  $I_{IN}$ ,  $V_{RN}$  is a white noise.

The last noise that we consider,  $R_{XN}$ , is often called excess noise, and it is due to resistance fluctuations. It is excess in the sense that resistors can be noisier than the Johnson noise formula predicts. This noise used to be called current noise because it requires a current through the resistors to detect it. However, the current does not produce the noise, and the association was misleading.<sup>13</sup> Good, low-noise component resistors may be obtained for  $R_f$ . For us the excess noise is due to the fluctuation of  $R_{sh}$  of the photodiode.

Excess noise includes the generation-recombination noise of semiconductors, which corresponds to fluctuations in the number of charge carriers.<sup>14</sup> This can be a white noise also. However the various factors that determine the I-V relationship of a diode<sup>15</sup> include the

mobility of the carriers as well as their number. Fluctuations of these other factors may cause  $1/f$  noise.<sup>16</sup>

When we fail to include excess noise in our circuit model it does not mean that this noise is insignificant or unimportant but only that it is unpredictable without a deeper knowledge of the inner workings of the photodiode. It may also vary because of environmental conditions, such as exposure of the photodiode to humid air.<sup>17</sup> Nevertheless, the circuit's response to photocurrent does not depend on  $R_{sh}$ , nor then to fluctuations in  $R_{sh}$ . These fluctuations matter in that they impose a noise voltage on the amplifier because of the amplifier's  $I_{Bias}$ .

Each of the four noise sources produces an independent, randomly varying voltage. The resistor noise  $V_{RN}$  can be directly measured at the amplifier output. The rms value of the total input noise voltage as seen by the amplifier is:

$$V_{IN} = [V_{VN}^2 + 4eI_{Bias}R_{so}^2\Delta f + (I_{Bias}R_{XN})^2] \quad (1a)$$

The sensitivity of the photocurrent measurement is limited by the total output noise voltage of the amplifier:

$$V_{ON} = [(A_V V_{IN})^2 + 4kTR_{so}\Delta f]^{1/2} \quad (1b)$$

where the closed loop voltage gain  $A_V$  is equal to  $(R_f + R_{sh})/R_{sh}$ .

This explains the critical importance of the photodiode shunt resistance in determining the ultimate sensitivity of the measuring circuit. To enable us to measure weak photocurrents,  $R_f$  must be made large. However, when  $R_f > R_{sh}$ , increasing  $R_f$  increases  $A_V$  significantly as well, implying an amplification of the noise along with the amplification of the signal. Larger values of  $R_{sh}$  permit larger values of  $R_f$  to increase amplification of the signal without undue noise.

### III. Measuring Voltage Noise

Before selecting a type of operational amplifier to be used for high-sensitivity applications, we independently measured the voltage noise of various candidates. Although bias current is often specified by the manufacturer, voltage noise, particularly at low frequencies, is a more subtle attribute. In this context, the noise is manifested as the scatter of repeated measurements of the amplifier's output offset voltage.

Output offset voltage is the nominal output value of the amplifier when no signal is applied and when the source resistance is low (so that input bias current effects are negligible). Like output voltage noise, it is usually proportional to  $A_V$ . The input offset voltage is the measured output offset voltage as reduced by this factor, and we take it to be an intrinsic amplifier characteristic. For this purpose, adjustment need not be made to reduce it.

Figure 2 shows the circuit used for these measurements as well as others that are discussed below. The circuit was enclosed in a lighttight and electrically shielded package. The amplifiers were installed in a socket for ease of substitution. Component resistors were sometimes substituted for the photodiode to rep-

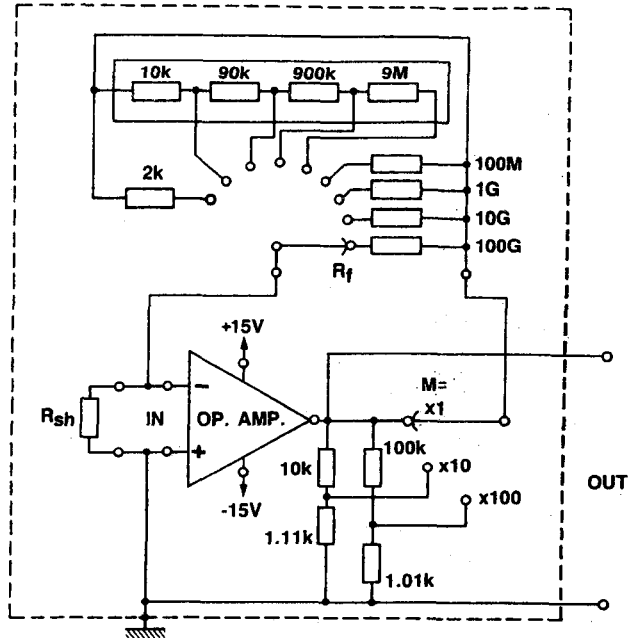


Fig. 2. Circuit details.

licate different source resistances. Both  $R_f$  and  $M$  were selected with switches. Here,  $M$  is a multiplier, an extra gain that could be introduced by reducing the feedback voltage through a resistive divider. This feature is appropriate only when  $R_f$  is well above the  $1-k\Omega$  output impedance of the divider.

[Whereas  $M$  may be used for amplifying the output from the detector, measurements showed that it does not improve the signal-to-noise ratio. Note that, while the signal gain is  $M \times R_f$ , the noise gain  $A_V$  is  $M \times (R_f + R_{sh})/R_{sh}$ . On the other hand, because the output of the amplifier remains bounded by the supply voltage, the dynamic range of the circuit is reduced when  $M > 1$ . Therefore the multiplication switch should be eliminated in most circumstances.]

The output of the circuit was connected directly to a microcomputer-controlled digital voltmeter (DVM). This multislope-type DVM integrated the output voltage for a selectable time period, a count of the power line cycles. To produce longer integration times than the DVM normally allowed, an external microcomputer averaged a sequence of repeated measurements.

Table I compares multiple samples of three types of operational amplifier from the Burr Brown product line. All are designed to be electrometer-type amplifiers, with a low input bias current. The OPA128LM and OPA104CM amplifiers are categorized as ultralow bias current devices. They are specified as having a bias current below 75 fA, the lowest of the product line. The OPA111BM amplifier has a higher bias current (specified as 1 pA, maximum) but is described as having lower noise. Nevertheless the manufacturer provides no specifications about noise below 0.1 Hz. Both the OPA128LM and the OPA111BM are newer generation products.

To measure the offset voltage and voltage noise of

**Table I. Statistics of Amplifier Output Measurements Showing the Mean (the Offset Voltage) and the Standard Deviation (the Voltage Noise)<sup>a</sup>**

Sample	OPA104CM		OPA128LM		OPA111BM	
	Mean	Std Dev	Mean	Std Dev	Mean	Std Dev
1	-23.84	7.94	-146.68	0.74	144.83	0.21
2	-36.81	9.10	67.24	0.53	-30.57	0.09
3	39.07	3.05	-111.02	0.55	-21.65	0.05
4	-79.14	8.27	158.66	1.30	-5.52	0.11
5	-107.05	6.71	30.19	0.42	—	—

<sup>a</sup> Values are quoted in millivolts, and the system gain  $A_V$  was 1000.

these candidate operational amplifiers, a 1-k $\Omega$  resistor was substituted for the photodiode to make the current and resistor noises negligibly small.  $R_f$  was set to 1 M $\Omega$ , and  $M = 1$  was used for an overall gain  $A_V$  of  $10^3$ .

The DVM was set to integrate for 100 power line cycles (10 cycles repeated 10 times and digitally averaged within the DVM). This integration time of 1.67 s would correspond to a measurement bandwidth for white noise of 0.3 Hz. One hundred of these readings were externally averaged, resulting in a single measurement of the output offset voltage. The measurement bandwidth for white noise in the latter case would be 1.25 mHz. The reason is explained in Appendix A.

The offset voltage was measured a nominal 10 times for each amplifier in this fashion, and the statistics of these 10 measurements are reported in Table I. The columns labeled Mean contain the results of final averaging of the 10 values. The columns labeled Std Dev contain the standard deviations of the 10 intermediate averages. The standard deviations of all 1000 individual readings were similar, showing that this noise was not much affected by the longer integration.

This behavior is indicative of  $1/f$  noise. A measurement passband depends on two characteristic times. The integration time of the individual data points determines the high-frequency rolloff, since the higher-frequency components are averaged out. Similarly the time spent making the repeated measurements determines the low-frequency rolloff, because lower-frequency components will not be noticed. That is, noise frequencies that act too slowly will not cause a scatter in the data during the time that one watches for it. Both rolloff frequencies are inversely proportional to their characteristic times in roughly the same way. For  $P$  quickly repeated measurements, the lower rolloff frequency is  $\sim 1/P$  of the higher.

For white noise with a large  $P$ , the measurement bandwidth is essentially determined by the upper rolloff frequency, as the difference between the lower rolloff and 0 Hz (i.e., dc) is small. Usually the lower rolloff frequency is ignored, and the noise is predicted by the integration time only. In contrast,  $1/f$  noise is more sensitive to the lower rolloff frequency. The rms voltage fluctuation owing to  $1/f$  noise goes as  $[\log(f_{\text{high}}/f_{\text{low}})]^{1/2}$ , the radicand being the number of decades in the noise passband. This equals  $[\log(P)]^{1/2}$ , a slowly varying function of  $P$ . Whereas data scatter caused by

white noise depends mostly on the integration time, data scatter caused by  $1/f$  noise depends mostly on the number of (equally timed) data points, independent of their integration time.

Here, if the noise were truly a  $1/f$  noise we would expect the standard deviation of the 1000 individual readings to be roughly  $\sqrt{3}$  times larger than that of the 10 intermediate averages. If it were a white noise instead, the standard deviation of the 10 intermediate averages would have been roughly  $\sqrt{240}$  times smaller, following the ratio of the bandwidths. Our data for the various amplifiers showed that the noise decreased by less than a factor of 2. Therefore, for simplicity in the remainder of this paper, input voltage noise will be treated as a constant, a characteristic of an amplifier, and independent of integration time. This relies on the slowly varying nature of  $[\log(P)]^{1/2}$  and says that the data in Table I ( $P = 10$ ) should be similar to the results obtained when  $10 < P < 30$ .

The data in Table I show that the OPA128LM amplifier has an order of magnitude less voltage noise than does the OPA104CM, the earlier generation amplifier having a consistently low noise level, used in our previous research.<sup>1</sup> However, on average the OPA128LMs' have approximately five times the voltage noise of the OPA111BM's.

Table I also shows noise variation among individual samples of OPA128LM amplifiers within a factor of 2 of the mean. This compares favorably with variations in other makes and models of operational amplifiers which, in our experience, can have noise levels that vary among samples by an order of magnitude. For most purposes this variation would not be significant, and individual selection of these amplifiers for low  $V_{VN}$  would not be necessary.

Also, please note that in product literature noise voltage is often reported peak to peak, not rms. As a rule of thumb, for 1000 measurements the peak-to-peak value will be  $\sim 6.6$  times larger than the rms one.<sup>18</sup>

#### IV. Temperature Dependence and Drift

It is not enough to develop new photodiodes with greater  $R_{sh}$  to achieve greater measurement sensitivity.  $R_{sh}$  and  $R_f$  affect the noise level in Eq. (1) through their combination,  $R_{so}$ . The current noise term is quadratic in  $R_{so}$ , and the resistor noise term depends on it linearly. As current noise becomes the dominant noise when  $R_{so}$  is large, care must be taken to use an amplifier with a sufficiently low  $I_{Bias}$ . Fortunately this is an easy criterion to meet. However, the bias current poses a greater problem because it changes with temperature. This is an aspect of the problem called drift.

In addition to random fluctuations (noise), there are also changes in the amplifier output that appear on inspection to be distinctively slower and often of larger magnitude. We interpret these changes as being caused by such things as the aging of the electronic components and their temperature dependence. We will elaborate on the latter effect for purposes of illustration and because it is the easiest source of drift to control. Drift is particularly bothersome in this re-

search because it may be confused with the low-frequency noise that we seek to compare.

As an example the manufacturer specifies that the OPA128LM amplifier has a typical input offset voltage  $V_O$  of  $\pm 140 \mu\text{V}$  ( $\pm 500 \mu\text{V}$ , maximum) and an input offset voltage drift  $V_D$  of  $\pm 5 \mu\text{V}/^\circ\text{C}$ . Its typical input bias current  $I_{\text{Bias}}$  is  $\pm 40 \text{ fA}$  (at  $25^\circ\text{C}$ ), and it grows geometrically at a rate  $I_D$  of  $6.7\%/^\circ\text{C}$ . (In light of the above discussion about input bias current noise, since the noise goes as the square root of the bias current the noise grows geometrically  $3.3\%/^\circ\text{C}$ .) In addition, we previously determined<sup>1</sup> the decrease of the photodiode shunt resistance with increasing temperature to be  $\sim 11\%/^\circ\text{C}$ , which we call  $R_{\text{SD}}$ . A nominal  $R_{\text{sh}}$  is  $5 \text{ G}\Omega$ . In the worst case,  $R_f$  is  $100 \text{ G}\Omega$ , with a negligible temperature dependence of  $< 500$  parts in  $10^6/^\circ\text{C}$ . These values lead to an  $A_V$  of 21, which increases  $11\%/^\circ\text{C}$ , and an  $R_{\text{so}}$  of  $4.8 \text{ G}\Omega$ , which decreases  $11\%/^\circ\text{C}$ .

Referring again to Fig. 1, we see the effect of  $V_O$  and  $I_{\text{Bias}}$  on the output voltage,

$$V_{\text{Offset}} = -A_V(V_O + I_{\text{Bias}}R_{\text{so}}). \quad (2)$$

For small temperature changes  $\Delta T$  with these typical component values,  $\Delta V_{\text{Offset}}/\Delta T = 0.7 \text{ mV}/^\circ\text{C}$  for the worst case alignment of the signs of  $V_D$ ,  $V_O$ , and  $I_{\text{Bias}}$ . In our experience, the value is closer to  $1.2 \text{ mV}/^\circ\text{C}$ , still well within specification limits.

It will simplify matters to cast the temperature effects in terms of a photocurrent change,  $\Delta I_{\text{Offset}}$ , that would yield an equivalent change in the magnitude of the output voltage. Because the photocurrent gain is  $R_f$ ,  $I_{\text{Offset}} = V_{\text{Offset}}/R_f$ , and

$$I_{\text{Offset}} = V_O/R_{\text{so}} + I_{\text{Bias}} \quad (3)$$

$$\Delta I_{\text{Offset}} = (V_D/R_{\text{so}} + V_O R_{\text{SD}}/R_{\text{so}} + I_D I_{\text{Bias}})\Delta T. \quad (4)$$

$\Delta T$  refers to the small temperature changes that occur during the course of a sequence of measurements.

Similarly noise may be expressed as the photocurrent that would give an equivalent deviation to the output voltage, on average:

$$I_{\text{Noise}} = V_{\text{ON}}/R_f = V_{\text{IN}}/R_{\text{so}}. \quad (5)$$

Of course, the detector–amplifier combination cannot effectively distinguish actual photocurrents smaller than these values. An appropriate design goal of the circuit is to equalize the effects of noise and drift, choosing an amplifier type that balances both problems for reasonable integration times and temperature control.

## V. Amplifier-Type Selection

Figure 3 predicts the performance of OPA111BM and OPA128LM amplifiers in this circuit. Drift and noise are computed by using Eqs. (4) and (5), respectively, and are shown as a function of source resistance  $R_{\text{so}}$ . The data for the typical amplifier characteristics are taken from the manufacturer's catalog, with the exception of  $V_{\text{VN}}$ , for which we use the average of the values in Table I. In the upper part of Fig. 3,  $\Delta T$  is  $0.1^\circ\text{C}$ , and  $\Delta f$  is  $300 \text{ mHz}$ . Both are easy to realize in an actual

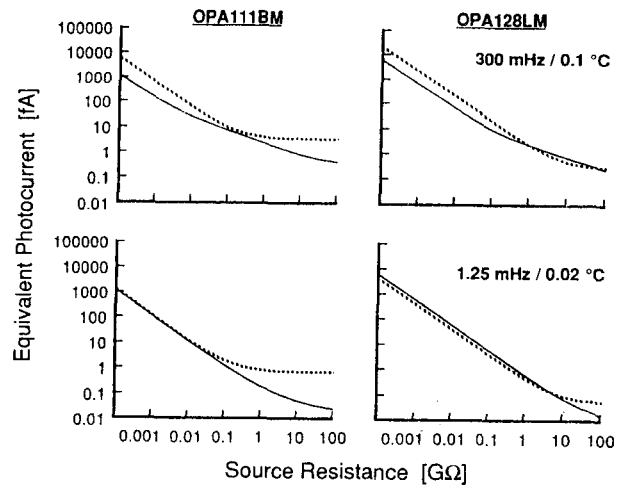


Fig. 3. Balancing noise and drift. The noise (solid curves) and thermal drift (dotted curves) are expressed in terms of the photocurrent that would cause an equal change in amplifier output. The two figures at the left show the expected performance of the OPA111BM amplifier; those on the right show the performance of the OPA128LM amplifier. The two top figures show easy specifications for integration time and temperature stability; the bottom two show tight specifications.

measurement. In the lower part of Fig. 3,  $\Delta T$  is  $0.02^\circ\text{C}$ , and  $\Delta f$  is  $1.25 \text{ mHz}$ .

Figure 3 shows that when  $R_{\text{so}} > 1 \text{ G}\Omega$  the most severe limit on sensitivity would be the drift caused by the temperature fluctuations of an OPA111BM amplifier. That is, the drift of the OPA111BM is much larger than both the noise and the drift of the OPA128LM. The last term of Eq. (4) is the culprit. For high-sensitivity investigations (when  $R_{\text{so}}$  must be large), it is generally better to choose an amplifier with low-input bias current (hence low bias current drift) than one with low voltage noise. However when  $R_{\text{so}} < 300 \text{ M}\Omega$ , the lower input offset voltage of the OPA111BM would provide the advantage. (Indeed in this situation it might be worthwhile to trim the amplifier to reduce  $V_O$ .)

There is an additional aspect to the combinations of  $\Delta f$  and  $\Delta T$  shown in Fig. 3. Photodiodes specially selected for high shunt resistance are available in the range of  $1\text{--}50 \text{ G}\Omega$ . In this range of source resistance, the noise and the drift that would result from the use of an OPA128LM amplifier are roughly equal. At the upper right of the figure, both  $\Delta f$  and  $\Delta T$  constrain the sensitivity of the detector electronics to  $\sim 1 \text{ fA}$ . A sensitivity of  $0.1 \text{ fA}$  requires reducing both  $\Delta f$  and  $\Delta T$  in tandem, as shown at the lower right, as well as a larger  $R_{\text{sh}}$ .

For the remainder of this paper we discuss results obtained while using OPA128LM amplifiers. The use of these amplifiers is consistent with the possibility of having excess detector noise, which would also be proportional to the input bias current.

## VI. Noise Characteristics of the Operational Amplifiers

Figure 4 shows noise measurements similar to those described in Section III made on OPA128LM amplifi-

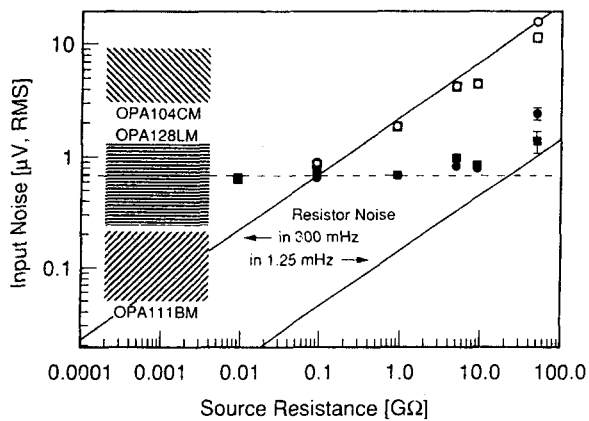


Fig. 4. Noise measurements of OPA128LM amplifiers with different source resistances. The hatched areas at the left show the range of the characteristic input voltage noises of the amplifier types reported in Table I. The dashed line guides the eye toward the voltage noise level of these particular amplifiers. This level of minimum noise cannot be much reduced by longer integration. The solid lines are the Johnson noise of the source resistances for our two integration times (300 mHz in open symbols and 1.25 mHz in filled symbols).

ers with various combinations of  $R_{sh}$  and  $R_f$  (both component resistors) at room temperature in a thermally insulated (but not regulated) box. This test determines whether the electrical noise from the electronics assembly is consistent with the predictions of the previous sections. The square data points were taken with one copy of the circuit, and the circular data points with another. The format parallels Eq. (1).

The DVM took 100 readings with integration times of 1.67 s. For each collection of 100 readings, the voltmeter reported their mean (measured in a bandwidth of 1.25 mHz) and their standard deviation (representing the noise in a bandwidth of 300 mHz). This cycle was repeated at least 40 times; sometimes the apparatus was run overnight and repeated the cycle  $\sim 140$  times.

The open points in Fig. 4 represent the total input noise [Eq. (1)] in a 300-mHz bandwidth. As before, the input noise is the measured (output) noise divided by  $A_V$ . The output noise is taken to be the average of the standard deviation reports from the voltmeter (each covering 100 individual readings). The single standard deviation of all the individual readings is not used in order to reduce the effect of long-term drift.

The filled points in Fig. 4 indicate the scatter of the means computed by the voltmeter. These points represent the total input noise in a bandwidth of 1.25 mHz. Nominally 30 consecutive readings were considered a group. However temperature-induced drift over the span of 30 measurements was a significant problem at large values of  $R_{so}$ . To reduce the effect of drift on the reported values, a least-squares fit was made to a line through the 30 consecutive values, and the implied time-dependent background was subtracted from the raw data. In effect, the noise below 1.25

mHz is taken to be the rms value of the residuals after the fit. The results of multiple sets of equal size were averaged when enough data were available.

The fitting procedure had the side effect of raising the low-frequency rolloff that affects the magnitude of  $1/f$  noise. It also narrowed the meaning of  $\Delta T$  in Eq. (4) to those temperature fluctuations that occurred on the time scale of a few measurements but not so slowly that they could be accounted for by background subtraction.

The resistor noise, as calculated at 300 K, is shown in Fig. 4 for the two bandwidths of interest. The ranges of voltage noises, as reported in Table I, are shown as shaded blocks at the left of the figure. This should be taken as a rough guide to the reproducibility of this experiment when other amplifiers of the same types are used. In our case, the two amplifiers used have very similar  $V_{VN}$  values. The dashed line represents an input voltage noise of  $0.68 \mu\text{V}$ . As expected for a bias current of only 75 fA, there is no evidence of current noise (noise proportional to  $R_{so}$ ) in this range of  $R_{so}$ . The voltage noise ( $1/f$  noise independent of  $R_{so}$ ) was remarkably consistent between the two bandwidths despite the different number of samples used and the differences in the way the data were treated.

The results show that the construction and the packaging of the complete amplifier circuits have not created an electrical noise much beyond that expected. At the longer integration time, the slight additional noise may be due either to temperature fluctuations  $>0.02^\circ\text{C}$  or to excess noise in the component resistors.

Finally note that in the viewpoint of Fig. 4 at a source resistance of 12 G $\Omega$ , the effects of voltage noise and resistor noise are equal in a measurement bandwidth of 1.25 mHz. The sensitivity of the circuit could not be readily improved there by simply integrating longer (which reduces resistor noise). Indeed, the shunt resistance of each photodiode implies an integration time that need not be exceeded.

## VII. Photodiode Noise

In this section we discuss noise measurements made when Hamamatsu photodiodes were used in the circuit. These diodes were specially manufactured and then selected for the highest shunt resistances that Hamamatsu could offer. The maximum  $R_{sh}$  requires the highest fabrication skill of the photodiode vendor and is limited by the number of crystal defects in the starting material. The type S1226-8BQ photodiode is a PNN<sup>+</sup> device; types S2386-8K and S2956-8BQ are made by P on N planar diffusion.

High-sensitivity applications suggest the use of large-area photodiodes to intercept more optical radiation. However with increasing area the shunt resistance is reduced, and the junction capacitance increases. To the extent that  $R_{sh}$  is due to leakage around the junction,  $R_{sh}$  will scale inversely by the square root of the diode's active area. To the extent that  $R_{sh}$  is an effect of the P-N junction itself,  $R_{sh}$  will scale inversely with the active area. The diodes used in this work all had active areas of  $1/3 \text{ cm}^2$ .

Table II. Noise and Drift of Complete Detector-Amplifier Packages Cast in Terms of the Photocurrent that Would Cause the Same Change in Output

Photodiode Type	$R_{sh}$ (G $\Omega$ )	$C_j$ (nF)	Circuit Copy	Limit Sensitivity (fA)	
				$\Delta f = 300$ mHz	$\Delta f = 1.25$ mHz
S1226-8BQ	6.5	1.3	A	$0.66 \pm 0.05$	$0.20 \pm 0.07$
S2956-8BQ	50	4	A	$1.0 \pm 1.2$	$0.16 \pm 0.05$
S1226-8BQ	8	1.3	B	$0.61 \pm 0.05$	$0.101 \pm 0.021$
S1226-8BQ	6.5	1.3	B	$0.61 \pm 0.05$	$0.102 \pm 0.015$
S2386-8K	20	3.2	B	$0.83 \pm 0.35$	$0.095 \pm 0.020$

We independently estimated the  $R_{sh}$  values of the photodiodes using a Hewlett-Packard 4145A semiconductor parameter analyzer to measure and display their I-V curves. Depending on the photodiode type, the highest shunt resistances available were in the range of 5–50 G $\Omega$ . These measurements have a tolerance of ~20% because the 4145A is not designed for such small currents. Additionally, these measurements are somewhat subjective, resulting from eyeball fits of the data with a visual guide provided on the screen of the analyzer.

When an actual photodiode is used in the circuit, the shunt impedance consists of the shunt resistance and a parallel junction capacitance. Because the shunt impedance is reduced at high frequencies, increased amplification of high-frequency noise will result. This can be compensated by adding parallel capacitance to the feedback resistor. We note the typical junction capacitance  $C_j$  of the various diodes. These data come from the manufacturer's catalog.

To determine the noise inherent in five different photodiodes, we used the procedure discussed in Section VI. The data are shown in Table II. Two different copies of the circuit were used. The B copy had a temperature monitor, which showed that the temperature was stable within 0.01°C during a 400-s measurement cycle. The reported uncertainties are due to the reproducibility of the measurements. They are the statistical standard deviation (1  $\sigma$ ) of >100 repeated measurements (consisting of 100 samples each) with 300-mHz bandwidth and 3 repeated measurements (consisting of 30 samples each) with 1.25-mHz bandwidth.

Note that the noise in  $\Delta f = 300$  mHz increases with increasing  $R_{sh}$  contrary to the expected trend. The scatter of the measurements increases as well. This is explained in part by noting that the RC time constants, which are of the order of 10–200 s, are much larger than the integration time of 1.6 s. The shunt impedance is reduced for noise frequencies within the detection bandpass, giving them extra amplification. With longer integration, the effect of junction capacitance is reduced.

The data show that noise-equivalent photocurrents of 0.1 fA have been achieved. This implies a dynamic range of 14 orders of magnitude for these devices since Hamamatsu specifies a saturation current of ~10 mA. (In practice, the OPA128LM amplifier can drive only 5 mA; a second-stage amplifier would be required for the full dynamic range.)

### VIII. Practical Considerations

In practice, the effect of long-term drift is mitigated by background subtraction. Each measurement should consist of a cycle containing intervals when the detector is exposed and when it is blocked. These periods of integration are separated by settling times, during which the output from the amplifier is ignored. When using the highest feedback resistor, 100 G $\Omega$ , we found that 2 min of settling was required for equilibrium to be reached. (This was considerably slower than the settling time for the 10-G $\Omega$  resistor, which was <1 s.)

In our experience, the maximum  $R_f$  that was suitable for the OPA128LM was 100 G $\Omega$ . For larger  $R_f$  the amplifier became noticeably nonlinear.

A fixed  $R_f$  of 100 G $\Omega$  gives the circuit a dynamic range of ~6 orders of magnitude. Note that 0.1 fA of photocurrent corresponds to an output voltage of 10  $\mu$ V, whereas the maximum output voltage is ~10 V, determined by the power supply. For field work, voltmeters with resolutions of 0.1 mV are readily available. With these, the minimum detectable photocurrent would be 1.0 fA, and the dynamic range would be one decade less.  $R_f$  values <100 G $\Omega$  might be appropriate depending on the brightness of the source.

It is customary to discuss noise in terms of the NEP incident upon a detector. Typical silicon photodiodes have a peak response of 0.4–0.6 A/incident W at approximately  $\lambda = 720$  nm. Here the NEP corresponding to 0.1 fA would be ~6 fW Hz<sup>-1/2</sup> (reflecting the 1-mHz bandwidth). 0.1 fA also corresponds to 780 photons/s for a diode with a typical external quantum efficiency of 80%.

### IX. Conclusion

For high-sensitivity applications, large-area (1/3 to 1 cm<sup>2</sup>) silicon photodiodes with high shunt resistance (>2 G $\Omega$ ) and little excess noise are the detectors of choice. They are best used in combination with an amplifier having the smallest possible input bias current because the high shunt resistance mitigates the input voltage noise. With the high-quality components now available, electrical noise can be reduced to an equivalent of 0.1 fA of photocurrent by using an integrated measurement time of 400 s. This is equivalent to a photocurrent caused by <800 photons/s, and it implies a dynamic range of 14 orders of magnitude for a detector circuit.

We have successfully built such a detector-amplifier package. While its NEP is comparable with that of

commercial offerings, the photodiode in our design has five times the active area.

Research continues at the National Institute of Standards and Technology to establish better the optical properties, such as their linearity over the whole dynamic range, of these detector circuits. Our goal is to package the circuits in a simple and practical manner and to calibrate them optically for distribution. We believe that these detector-based transfer standards will serve the needs of the radiometric community for traceability to the National Institute of Standards and Technology's primary standards, which serve a more limited dynamic range. In addition, the spectral response of the detector may be customized by the addition of a colored filter for special applications, such as in photometry.

Beyond their application in standards research, the improved performance of the detectors now possible should find them application in many areas of commercial interest. Of particular note is the band of near-infrared wavelengths between 700 and 1000 nm, where photomultiplier tubes are generally less efficient and require noisy photocathodes. However the relative simplicity and lower cost of high-sensitivity, silicon photodiode detectors might make them more appropriate than photomultiplier tubes, even for visible light, in many circumstances. We hope that as photodiode manufacturers become more aware of the significance of a high shunt resistance, devices featuring this characteristic will become more widely available.

#### Appendix A: Determining the Measurement Bandwidth

The magnitude of the white noise discussed in Section II was dependent on the bandwidth of the measurement. Although it is commonly known that the bandwidth  $\Delta f$  is inversely proportional to the integration time  $\tau$  of a system, the value of the proportionality constant is the source of perpetual confusion.

Consider a signal, which need not be noisy, which we shall call  $f(t)$ . In our case, this signal is the output voltage of our amplifier circuit. By integration of this signal we mean a transformation to another signal,  $f'(t)$ , which could be, for example, either of the following:

$$f'(t) = \frac{1}{\tau} \int_{t-\tau}^t f(t') dt' \quad (\text{Case I}), \quad (\text{A1})$$

$$f'(t) = \frac{1}{\tau} \int_{-\infty}^t \exp\left[-\frac{(t-t')}{\tau}\right] f(t') dt' \quad (\text{Case II}). \quad (\text{A2})$$

In each of these cases the integration, expressed as a convolution integral, is an averaging with a particular weighting function. The first case is pure integration over a finite time interval. It is the continuous analog to the practice of digitally averaging a certain number of the most recent points. The second case is that of a simple, single-pole filter.

Consider now the effect of these time-domain filters upon a signal  $f(t) = e^{-i\omega t}$ . After integration

$$f'(t) = \left( \frac{e^{i\omega\tau} - 1}{i\omega\tau} \right) e^{-i\omega t} \quad (\text{Case I}), \quad (\text{A3})$$

$$f'(t) = \left( \frac{1}{1 - i\omega\tau} \right) e^{-i\omega t}. \quad (\text{Case II}). \quad (\text{A4})$$

The expressions in parentheses correspond to attenuations in the frequency domain due to the filters [Eqs. (A1) and (A2)] in the time domain. Note that they approach 1 for small  $\omega$  and that their magnitudes approach 0 for large  $\omega$ . They are perhaps best recognized as the Fourier transformations of the weighting functions.

For a signal  $f(t)$  that contains white noise, there is equal noise power in all intervals of  $\omega$  and in both quadrature phases. Therefore the attenuation in Eq. (A3) or (A4) would have the same effect on white-noise power as an equivalent frequency-domain attenuator that is 1 over an interval  $\Delta\omega$  and 0 elsewhere, where  $\Delta\omega$  is the integral of the squared magnitude of the (voltage) attenuation over all frequencies:

$$\Delta\omega = \int_0^{\infty} \frac{2[1 - \cos(\omega\tau)]}{(\omega\tau)^2} d\omega = \frac{\pi}{\tau} \quad (\text{Case I}), \quad (\text{A5})$$

$$\Delta\omega = \int_0^{\infty} \frac{1}{1 + (\omega\tau)^2} d\omega = \frac{\pi}{2\tau} \quad (\text{Case II}), \quad (\text{A6})$$

As  $\omega = 2\pi f$ ,  $\Delta f = 1/(2\tau)$  in Case I, and  $\Delta f = 1/(4\tau)$  in Case II. That is, the value of the proportionality constant depends on the details of what makes up the integration time,  $\tau$ . Here the two different results reflect the fact that it takes more high frequencies to represent an abrupt function of time than a gradual one.

There are, of course, many other low-pass filters that commercial dc voltmeters might use. One does not know *a priori* what the proportionality should be between  $\Delta f$  and  $1/\tau$ .

In this research we used Hewlett-Packard Models 3456A and 3457A voltmeters. Their analog-to-digital converters use variations of the well-known dual-slope technique. However for long integration times, successive samples made with shorter integration times are digitally averaged. The upramp portion of a single analog-to-digital cycle consists of the integration described in Eq. (A1), with  $\tau = 0.167$  s (10 power line cycles). These are repeated  $N$  times,  $T = 0.4$  s apart (for the 3457A; 0.34 s for the 3456A).

The bandwidth of this class of instrument is

$$\Delta\omega = \int_0^{\infty} \left\{ \frac{2[1 - \cos(\omega\tau)]}{(\omega\tau)^2} \right\} \left\{ \frac{[1 - \cos(N\omega T)]}{N^2[1 - \cos(\omega T)]} \right\} d\omega. \quad (\text{A7})$$

This follows directly from the choice of a weighting function [as in Eqs. (A1) and (A2)] that is a sequence of  $N$  square pulses each with amplitude  $1/N$ . Equation (A1) is the special case with  $N = 1$ , and the first factor in the integrand of Eq. (A7) parallels the integrand in Eq. (A5). Using the well-known property of Fourier transforms that the transform of a convolution is the product of the transforms of its constituents, we recognize the second factor in Eq. (A7) as the squared magnitude of the transform of a sequence of  $N$  delta functions (impulses).

We have confirmed the behavior of this expression by numerical integration. In the low- $N$  limit ( $N < 30$ )

for these  $\tau$  and  $T$ ),  $\Delta f \approx 1/(2N\tau)$ . In the high- $N$  limit ( $N > 1000$  for these  $\tau$  and  $T$ ),  $\Delta f \approx 1/(2NT)$ .

In this paper a bandwidth of 0.3 Hz refers to a panel setting on an HP 3457A of 100 power line cycles (1.67 s) of integration time. Internally the HP 3457A implements this as  $\tau = 0.167$  and  $N = 10$ . A bandwidth of 1.25 mHz refers to panel settings of 100 power line cycles repeated 100 times. While the integration time is 166.7 s, as  $N = 1000$  in this case, the elapsed time of 400 s determines the bandwidth.

Incidentally, nothing in the preceding analysis is connected with the problem of detecting low noise frequencies. When trying to measure the noise by determining the scatter (standard deviation) of many samples, noise at low frequencies is not resolvable from the signal (the mean). Just as  $\tau$  provided a characteristic time that determined the upper bound of the passband, the total time  $T$  spent making measurements provides the characteristic time for the lower bound. The actual bandwidth when we are trying to measure white noise is  $(1 - C\tau/T)\Delta f$ , where  $C$  is a constant of order unity (and which depends on the details of the measurements). Nevertheless  $\Delta f$  is still the bandwidth that reflects the statistical uncertainty in a real signal that is due to the noise.

The authors thank Joel Fowler, Jon Geist, and Ed Zalewski for the encouragement that started this project, Steve Southworth for sharing his valuable experiences in the use of these detector circuits, Tom Larson for the long hours spent measuring the noise, Alan Migdall for many helpful discussions on the nature of the noise, Raju Datla for a careful reading of the manuscript, and Al Parr, Klaus Mielenz, and Chris Kuyatt for their assistance and support.

## References and Notes

- G. Eppeldauer, "Measurement of very low light intensities by photovoltaic cells," in *Eleventh International Symposium on Photon Detectors, Weimar (GDR), 1984*, Proc. 182 (IMEKO, Budapest, 1984).
- Data sheet of the HC210-3314 and HC212-3314, "Integrated silicon photodiode and amplifier for low light level detection," (Hamamatsu Corp., 1988).
- W. Budde, "Multidecade linearity measurements on Si photodiodes," *Appl. Opt.* **18**, 1555-1558 (1979).
- W. J. Borucki, "Photometric precision needed for planetary detection," in *Proceedings of the Workshop on Improvements to Photometry, San Diego, 1984*, NASA Conf. Publ. CP-2350, 15-27 (1984); W. J. Borucki and A. L. Summers, "The photometric method of detecting other planetary systems," *Icarus* **58**, 121-134 (1984).
- G. Eppeldauer and A. R. Schaefer, "Application of PN and avalanche silicon photodiodes to low-level optical radiation measurements," in *Second Workshop on Improvements to Photometry, Gaithersburg, 1987*, NASA Conf. Publ. CP-10015, 111-151 (1988).
- E. F. Zalewski and J. Geist, "Silicon photodiode absolute spectral response self-calibration," *Appl. Opt.* **19**, 1214-1216 (1980).
- A. R. Schaefer, E. F. Zalewski, and J. Geist, "Silicon detector nonlinearity and related effects," *Appl. Opt.* **22**, 1232-1236 (1983).
- J. L. Gardner and F. J. Wilkinson, "Response time and linearity of inversion layer silicon photodiodes," *Appl. Opt.* **24**, 1531-1534 (1985).
- E. F. Zalewski and C. R. Duda, "Silicon photodiode device with 100% external quantum efficiency," *Appl. Opt.* **22**, 2867-2873 (1983).
- C. L. Wyatt, *Radiometric System Design* (Macmillan, New York, 1987), Chap. 18.
- A. Ambrózy, *Electronic Noise* (McGraw Hill, New York, 1982), p. 190.
- It is incorrect to say that the shunt resistance, defined as  $dV/dI$  at the operating point, is the effective resistance for thermal noise in the Johnson-Nyquist equation. However for the well-known exponential I-V relation of a junction diode, it is an appropriate approximation when the diode current is much less than its reverse saturation current. That is the case in this research, where  $I_s \approx 5$  pA and  $I \approx 0.05$  pA owing to the op-amp input bias current. In general, the effective resistance (and hence the noise generated) will be less, approaching  $1/2 dV/dI$  when  $I \gg I_s$ ; see Eq. (19) in M. S. Gupta, "Thermal noise in nonlinear resistive devices and its circuit representation," *Proc. Inst. Electr. Eng.* **70**, 788-804 (1982).
- K. M. van Vliet, "Classification of noise phenomena," in *Sixth International Conference on Noise in Physical Systems, Gaithersburg, 1981*, Natl. Bur. Stand. (U.S.) Tech. Note **614**, 3-11 (1981).
- R. Müller, "Generation-recombination noise," in *Noise in Physical Systems, Proceedings of the Fifth International Conference on Noise, Bad Nauheim (FRG), 1978* (Springer-Verlag, New York, 1978).
- S. M. Sze, *The Physics of Semiconductor Devices*, 2nd ed. (Wiley, New York, 1981), Chap. 2.
- See, e.g., D. A. Bell, "The role of mobility in  $1/f$  noise" in *Sixth International Conference on Noise in Physical Systems, Gaithersburg, 1981*, Natl. Bur. Stand. (U.S.) Tech. Note **614**, 169-172 (1981); R. P. Jindal and A. Van der Ziel, "A model for  $1/f$  mobility fluctuations in elemental semiconductors," *ibid.*, 173-177; B. K. Jones, "Excess conduction noise in silicon resistors," *ibid.*, 206-209.
- G. L. Pearson, H. C. Montgomery, and W. L. Feldmann, "Noise in silicon p-n junction photocells," *J. Appl. Phys.* **27**, 91-92 (1956).
- Linear Products Databook* (Analog Devices, Inc., 1988), pp. 2-9.